Surface & Coatings Technology 272 (2015) 298–308

Contents lists available at ScienceDirect

Surface & Coatings Technology

journal homepage: www.elsevier.com/locate/surfcoat

Effect of plasma nitriding on the strength of fine protrusions formed by sputter etching of AISI type 420 stainless steel

Keijiro Nakasa [a,*], Akihiro Yamamoto [b], Rongguang Wang [c], Tsunetaka Sumomogi [d]

[a] High-Tech Research Center, Hiroshima Kokusai Gakuin University, 6-20-1 Aki-ku, Hiroshima 739-0321, Japan
[b] Asahi Surface Tec LLC, 648-16 Misono, Saijo-cho, Higashi-Hiroshima 739-0024, Japan
[c] Department of Mechanical Systems Engineering, Faculty of Engineering, Hiroshima Institute of Technology, 2-1-1 Miyake, Saeki-ku, Hiroshima 731-5193, Japan
[d] Department of Manufacturing Engineering, Faculty of Engineering, Hiroshima Kokusai Gakuin University, 6-20-1 Aki-ku, Hiroshima 739-0321, Japan

ARTICLE INFO

Article history:
Received 17 December 2014
Accepted in revised form 28 March 2015
Available online 4 April 2015

Keywords:
Plasma nitriding
Protrusion
Sputter etching
Type 420 steel
Hardness test
Scratch test

ABSTRACT

Argon ion sputter-etching of AISI type 420 martensitic stainless steel was carried out to form conical protrusions with bottom diameter of 10–30 μm on the specimen surface by using a radio-frequency magnetron sputter-apparatus. Plasma-nitriding was applied to the protrusions with various mixing rate of nitrogen and argon gas. The shape of the protrusions was examined by using a scanning electron microscope, and the nitrides formed on the protrusions were identified by means of an X-ray diffraction analysis. Micro-Vickers hardness tests and nano-scratch tests were used to evaluate the deformation resistance of the protrusions. By plasma-nitriding at a nitrogen pressure of 130 Pa and a nitriding power of 50 W, about 1.3 times larger indentation resistance than that of the as-sputter-etched protrusions was obtained after a long nitriding time of 14 ks. When plasma-nitriding was carried out at a lower nitrogen pressure of 1.2 Pa and a higher nitriding power of 200 W for 7.2 ks, indentation and scratch resistances of the protrusions largely increased to the values almost three times as large as those of the as-sputter-etched protrusions. However, the protrusions were brittle due to the formation of thick nitride layers and the sharpness of the protrusions was lost. Reduction of the nitriding power to 50 W recovered the sharpness with small amount of surface nitride layer, but the indentation resistances were only 1.4 times larger values than those of the as-sputter-etched protrusions. On the other hand, plasma-nitriding using a mixture of nitrogen gas of 0.53 Pa and argon gas of 0.67 Pa at the power of 50 W produced almost twice larger indentation and scratch resistances than those of the as-sputter-etched protrusions within a short nitriding time of 1.8 ks, retaining the sharpness of protrusions without forming brittle nitrided layers.

1. Introduction

Surface textures with fine protrusions have been attracting the interests of many researchers and engineers due to their unique functions covering physical, optical, electronic and chemical areas. Examples of the functions are high absorbance of visible light (moth-eye structure) [1–3], super-hydrophobicity (lotus-effect) and super-hydrophilicity [4–6], structural colors of plants and insects [7], and high electron emission [8] due to sharp tips of the protrusions. Whatever functions are utilized in engineering products, the mechanical functions, such as strength, ductility and wear-, heat-, and corrosion-resistance of protrusions, are important to maintain the functions for long period.

The strong protrusions are also desirable exclusively for mechanical uses depending on their sizes. For example, protrusions with 300–800 nm sizes can be used as dies or rolls to fabricate the moth-eye structure for anti-reflecting camera lens or films for a television display. On the other hand, high and sharp protrusions with bottom sizes of 1–100 μm or more are desirable for the following uses: (1) large and sharp protrusions can be used as a traction roll to carry sheet, cloth, paper, food and other soft materials even in a slippery liquid environment where an optimum protrusion size should be selected in order to obtain high friction force but not to damage the surface of materials, (2) sharp and dense protrusions can be used as transcription roll or die to give many holes onto polymer sheets for low reflectance of visible light or high adhesion of paint, where too small protrusions are of no use due to high deformation recovery of polymers, (3) a couple of plates with hard protrusions and harder smooth surface can be utilized as a low frictional sliding pair, the spaces among which are filled by liquid or solid lubricant, and (4) strong anchor effect of protrusions is used as a substrate to deposit thick wear-, heat- or corrosion-resistant film.

One of the methods to fabricate various sizes of fine protrusions is the sputter- or plasma-etching of metals [9] where fine precipitates, inclusions and alloying or impurity atoms with low sputter-rate give origins of protrusions. The size and shape of protrusions can be controlled by using a mask and photolithographic technique [1,8] or

* Corresponding author. Tel.: +81 82 820 2653; fax: +81 82 820 2654.
E-mail addresses: nakasa@hkg.ac.jp (K. Nakasa), yamamoto@gmail.com (A. Yamamoto), wangrg@cc.it-hiroshima.ac.jp (R. Wang), sumomogi@hkg.ac.jp (T. Sumomogi).

http://dx.doi.org/10.1016/j.surfcoat.2015.03.048
0257-8972/

by putting powders on the substrate as seeds instead of the mask [10]. The present authors have already applied sputter-etching to commercially supplied steels and showed that high density of cone- or column-shaped protrusions ranging from nano- to micron-meter sizes are automatically formed although the heights, sizes and shapes of the protrusions are not necessarily regular. For type H21, H13 and M2 tool steels containing W, Cr, Mo, and V elements [11–15] or type 316 and 316 L stainless steels [13–15] the cone- or column-like protrusions with nano-meter sizes are formed, whereas the conical protrusions with micron-meter sizes are formed for type 304 austenitic stainless steel [16–19], type 430 ferritic and type 410, 420 and 440C martensitic stainless steels [19,20]. Because this technique only uses argon gas and commercially supplied steels without using masks or seed powders and special etching gas, the production cost is much lower than that of other methods.

According to our previous research, the protrusions formed on the stainless steels with sizes of more than 5 μm revealed excellent mechanical functions, such as anchor effect [18], compressive and scratch strength [19], corrosion resistance [16] and delamination strength even by large plastic deformation of substrate [17]. For further enhancement of mechanical properties, surface modification of the protrusions is necessary. The authors [20] have already reported that the indentation resistance of the protrusions formed on type 420 martensitic stainless steels is increased by quenching. One of the other efficient and effective methods is plasma-nitriding because the same apparatus as is used for sputter-etching can be utilized to subsequent nitriding process and it is applicable to all the steels even to a steel with low carbon content.

There are so many researches on the application of plasma-nitriding to smooth surface of steels including Cr–Mo steel [21], austenitic stainless steels [22–27] and ferritic or martensitic stainless steels [28–32]. As is well known, a large increase in surface roughness occurs due to sputter effect of nitrogen ions and/or formation of brittle ε-$Fe_{2-3}N$ layer during plasma-nitriding process. In a usual machine part the brittle and rough nitrided surface is ground away, and the underlying hard γ′-Fe_4N layer and diffusion layer including fine precipitates of nitrides contribute to wear resistance. However, such a mechanical polishing is not applicable to fine protrusions. Thus, in a worst case, the sharpness and ductility of the protrusions could be lost by plasma-nitriding. On the other hand, low temperature plasma-nitriding has been applied to austenitic stainless steels to obtain higher corrosion resistance with relatively high hardness [22–27]. In this treatment, so-called γ_N- or S-phase, which is composed of γ-solid solution with high nitrogen content or, in some case, with very fine nitride precipitates, appears without forming thick nitrided layers although the surface roughness occurs even in low temperature plasma-nitriding [27]. Low temperature plasma-nitriding has been already applied also to type 410 and 420 martensitic stainless steels [30–32].

In the present research, considering the application of protrusions to the traction and transcription rolls mentioned above, plasma-nitriding was carried out on the protrusions formed by sputter-etching of type 420 martensitic stainless steel. The reason for the selection of this steel is that sharp cone-shaped protrusions with bottom diameter of more than 10 μm are stably formed [20].

2. Experiment method

2.1. Preparation of specimen and sputter-etching

The material used is AISI type 420 (JIS: SUS420J2) martensitic stainless steel. The chemical composition of the steel (mass %) is; C: 0.35, Si: 0.55, Mn: 0.45, P: 0.025, S: 0.016, Ni: 0.22, Cr: 12.27, and Fe: Bal. The as-received steel bar with 10 mm diameter was cut to a disk of 1.5 mm thickness by using a wire-cutting electrical discharge machine. Specimen surface was polished by using emery papers up to #1000 and ultrasonically cleaned in ethyl-alcohol. Then the specimens were set on a type 304 stainless steel disk of 100 mm diameter and 3 mm thickness on the Cu cathode electrode of an RF magnetron sputtering apparatus (Sanvac Co.: SP300(M)). After vacuum pressure reached a value lower than 6×10^{-3} Pa, argon gas (purity: 99.999%) was introduced and maintained at a pressure of 0.67 Pa. Sputter-etching of the specimens was carried out at a sputter power of 250 W and a current smaller than 200 mA. With increasing sputter-etching time the size of protrusion increases and the protrusion surface remains smooth until 11 ks [20]. With further increase in sputter-etching time, surface roughness of the protrusions gradually increases. The rough surface of the protrusions may be useful to increase the anchor effect of coated film, whereas the smooth surface is desired for the traction roll in order not to damage the materials and also for the transcription roll in order to decrease the transcription force. In the present research, the sputter-etching time of 9 or 11 ks was selected to obtain the protrusions with smooth surface.

Generally, a machine part made of martensitic stainless steel is quenched and tempered before plasma-nitriding, and the plasma-nitriding temperature should be lower than the tempering temperature of this steel (873–1023 K). However, in the present research, heat treatments of the specimens were not carried out. The reason is that the temperature of protrusions increases to a higher temperature, e.g. 1073 K [20], by the sputter-etching of the protrusions with large surface area but small volume, and the high temperature continues for long time of 9–11 ks. Even if the heat treatments were applied, hardness should have been lost before nitriding.

2.2. Plasma-nitriding conditions

Usually, an industrial plasma-nitriding is carried out by using a direct-current (DC) plasma introducing a mixture of nitrogen and hydrogen gases at a pressure between 100–1000 Pa, where an abnormal glow discharging occurs between both electrodes. However, this process needs very long nitriding time, e.g. 36 ks (10 h)–108 ks (30 h) for the formation of hard layer. On the other hand, the RF magnetron sputter apparatus as is used in the present research has been originally developed to obtain high sputter efficiency of a target material under a low argon gas pressure smaller than 1 Pa. In the RF magnetron sputter apparatus, ionizing efficiency of nitrogen gas is much larger than that in the DC plasma and the nitrogen ions impinge onto the surface with much higher speed than that in the DC plasma. So that, even if the nitrogen gas pressure is increased, collision between nitrogen ions increases whereas impingement speed of nitrogen ions on the specimen surface decreases. Thus similar plasma-nitriding conditions to those in DC plasma-nitriding cannot be applied in RF-plasma nitriding. In addition, it seems that there is no need to add hydrogen gas to nitrogen gas because the surface oxide layer to be reduced by hydrogen has not been formed during the sputter-etching just before nitriding.

There seems to be no literature that has reported plasma-nitriding of protrusions using the RF magnetron sputter apparatus. Thus, the experiments were carried out changing the nitrogen gas pressure, a mixing rate of argon gas, sputter power and sputter time as are classified in Table 1. In group 1, the plasma-nitriding is carried out only by using nitrogen gas (purity: 99.999%) of 130 Pa, which is the lowest pressure level for DC plasma-nitriding but will be very high for RF-magnetron nitriding, at a sputter power of 50 or 100 W for 7.2 ks or 14 ks. The specimens nitrided with these conditions are called, e.g. $N_2$130 Pa–50 W–7.2 ks specimen, $N_2$130 Pa–100 W–7.2 ks specimen, or $N_2$130 Pa–(50, 100)W–7.2 ks specimens together. The reason for much shorter nitriding time than the conventional DC plasma-nitriding time is that the nitride layers should be limited only on protrusion surface even if they are formed. However, from the experimental results as is described later, the indentation resistance of protrusions was only 1.3 times as large as that of the as-sputter-etched protrusions even for the nitriding time of 14 ks. So that the second process classified as group 2 was tried by decreasing the

Table 1
Plasma nitriding conditions and comparison of top sharpness and scratch ductility of protrusions. The mark # indicates the scratch ductility obtained from nano-scratch test. A: very high, B: high, C: low, D: very low.

Group	Specimen name	N_2 pressure (Pa)	Ar pressure (Pa)	Power (W)	Time (ks)	Top sharpness	Scratch ductility
0	As-sputter-etched	0	0.67	250	11	A	#A (Fig. 9)
1	$N_2$130Pa–50 W–7.2 ks	130	0	50	7.2	A	A(Fig. 13(a))
	$N_2$130Pa–50 W–14 ks			50	14	A	A
	$N_2$130Pa–100 W–7.2 ks			100	7.2	A	A
2	$N_2$1.2 Pa–50 W–1.8 ks	1.2	0	50	1.8	A	A
	$N_2$1.2 Pa–50 W–3.6 ks			50	3.6	A	A
	$N_2$1.2 Pa–50 W–7.2 ks			50	7.2	A	A(Fig. 13(b))
	$N_2$1.2 Pa–100 W–1.8 ks			100	1.8	B	C
	$N_2$1.2 Pa–100 W–7.2 ks			100	7.2	B	C (Fig. 13(c))
	$N_2$1.2 Pa–200 W–7.2 ks			200	7.2	D	#D (Fig. 10)
	$N_2$1.2 Pa–Ar0.67 Pa–200 W–1.8 ks		0.67	200	1.8	D	D
3	$N_2$0.53 Pa–Ar0.67 Pa–50 W–1.8 ks	0.53	0.67	50	1.8	A	#B (Fig. 11)
	$N_2$0.53 Pa–Ar0.67 Pa–50 W–7.2 ks			50	7.2	A	B
	$N_2$0.53 Pa–Ar0.67 Pa–100 W–1.8 ks			100	1.8	B	C
	$N_2$0.53 Pa–Ar0.67 Pa–200 W–1.8 ks			200	1.8	D	D

nitrogen pressure to 1.2 Pa. Although the indentation resistance largely increased in the $N_2$1.2 Pa-(100, 200)W-7.2 ks specimens, the nitriding power of 100 and 200 W eventually resulted in a loss of sharpness and formation of brittle nitrides on the protrusions. Reduction of the nitriding power to 50 W suppressed the nitride formation but the indentation resistance was still about 1.4 times as large as that of the as-sputter-etched specimen. Finally, the third nitriding processes of group 3 were tried at a lower nitrogen gas pressure of 0.53 Pa mixed with argon gas of 0.67 Pa; $N_2$0.53 Pa–Ar0.67 Pa–50 W–1.8 ks specimen, etc.

2.3. Analyses of nitrided layer and evaluation of strength of protrusions

Morphologies of specimen surfaces after the sputter-etching or plasma-nitriding were observed by a scanning electron microscope (SEM) (JEOL, JSM-6510A) with an accelerating voltage of 15 kV, work distance of 9–19 mm and a spot size of 50 nm. Nitrides formed on the protrusion surface were identified by an X-ray diffractometer (Rigaku, RINT-2200) using a Cu X-ray tube under the operating voltage of 40 kV and current of 40 mA. The scattering and receiving slit widths were 1.26 and 0.3 mm, respectively, and the scan speed of X-ray counter was 0.017°/s. Cross-section of the protrusion was observed by using an optical microscope after etching by 5% nital, and an EDX analysis was carried out to confirm the existence of chromium and nitrogen atoms in each nitride layer. The deformation resistance of the protrusions to indentation force (indentation resistance) was measured by using a micro-Vickers hardness tester (Shimadzu, type B) with an indentation force of 2.9 N and a holding time of 30 s. The resistance to scratch force (scratch resistance) was evaluated using a nano-scratch tester (CSM Instruments, sphero-conical diamond indenter with tip radius of 10 μm) under the loading speed of 0.17 mN/s and scratch speed of 16.7 μm/s for scratch distance of 5 mm.

3. Results and discussions

3.1. Effect of plasma-nitriding on the shape of protrusions

Fig. 1 shows an example of SEM images of the protrusions formed by the sputter-etching at 250 W for 11 ks before plasma-nitriding. The protrusions are cone-shaped with sharp top and the average bottom size of the cones is more than 20 μm. Fig. 2 shows examples of SEM images after the plasma-nitriding of the protrusions. The protrusions of $N_2$130 Pa–50 W–14 ks specimen (a) of group 1 in Table 1 are sharp. Although the protrusions of the $N_2$1.2 Pa–50 W–1.8 ks specimen (b) in group 2 have sharp tops and the $N_2$1.2 Pa–100 W–7.2 ks specimen (c) barely keeps the sharpness, the $N_2$1.2 Pa–200 W–7.2 ks specimen (d) has lost the original sharpness of protrusions. In addition, the protrusion surface of these $N_2$1.2 Pa–(100, 200)W–7.2 ks specimens is coarse compared with that of the as-sputter-etched specimen (Fig. 1), the $N_2$130 Pa–50 W–14 ks (a) and $N_2$1.2 Pa–50 W–7.2 ks (b) specimens. The $N_2$0.53 Pa–Ar0.67 Pa–50 W–1.8 ks (e) and $N_2$0.53 Pa–Ar0.67 Pa–50 W–7.2 ks specimens (f) in group 3 keep high sharpness and smooth surface of protrusions.

The sharpness of the protrusions of all the specimens is summarized in Table 1 with ranks from A (very high) to D (very low). The aspect ratio of height to diameter of protrusions (a, b, c, e, and f) is almost the same as that of the as-sputter-etched protrusion (Fig. 1), whereas it is smaller for the protrusions sputter-etched at 200 W (d). From Table 1 and Fig. 2, it is concluded that common features of dull tops and rough surface appear when the sputter power is 100 and 200 W,

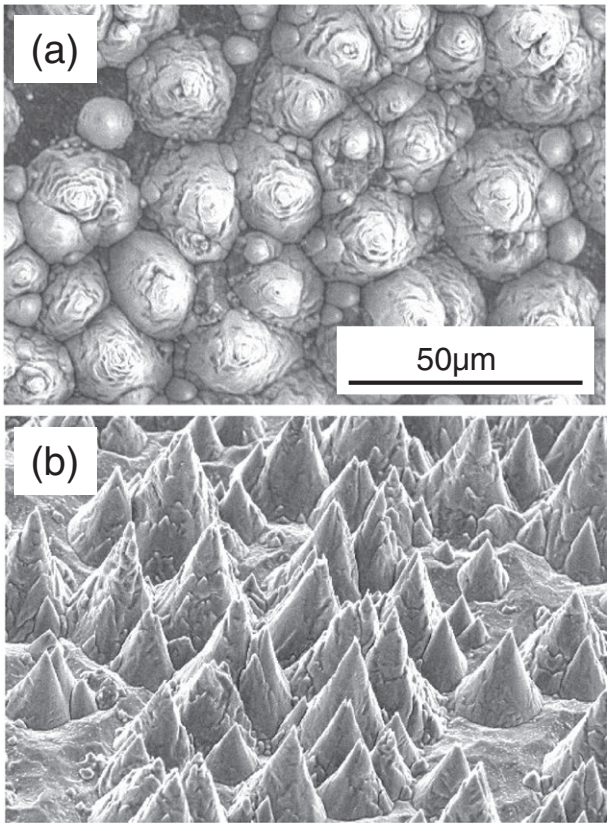

Fig. 1. SEM images of conical protrusions formed by sputter-etching at 250 W for 11 ks (as-sputter-etched specimen). (a) is top view and (b) is 45° inclined side view.

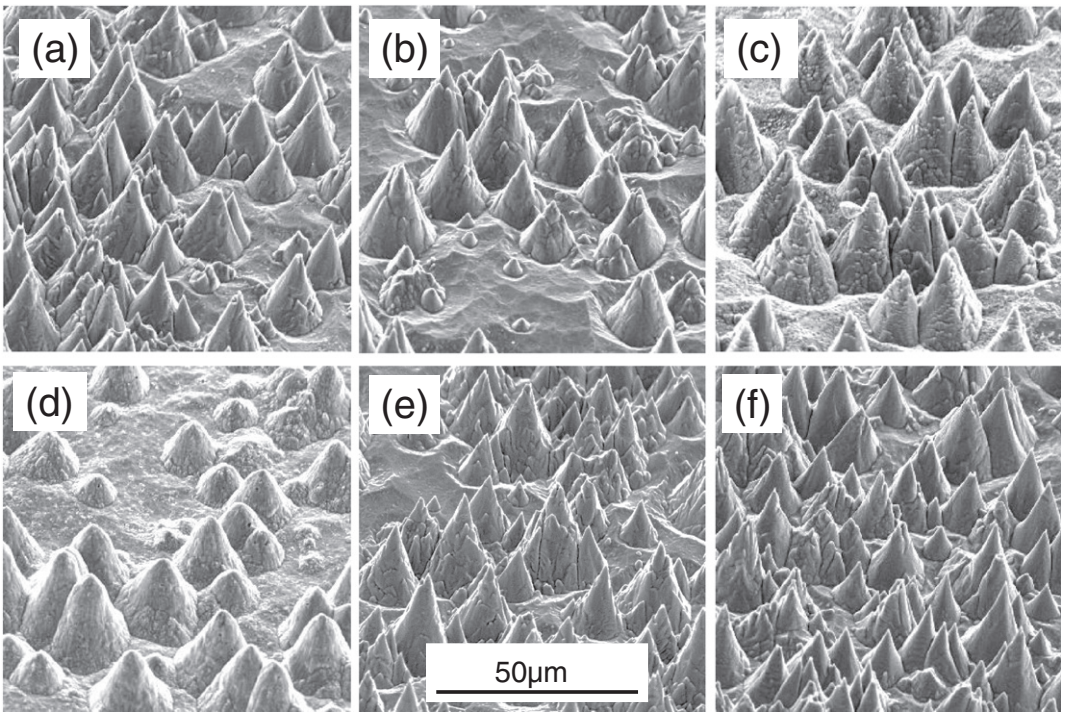

Fig. 2. Plasma-nitrided protrusions of $N_2$130Pa–50 W–14 ks specimen (a), $N_2$1.2 Pa–50 W–7.2 ks specimen (b), $N_2$1.2 Pa–100 W–7.2 ks specimen (c), $N_2$1.2 Pa–200 W–7.2 ks specimen (d), $N_2$0.53 Pa–Ar0.67 Pa-50 W–1.8 ks specimen (e) and $N_2$0.53 Pa–Ar0.67 Pa-50 W–7.2 ks specimen (f). Scales are all the same.

and the low aspect ratio of height to diameter appears when the sputter power is 200 W. This means that the nitrogen ion sputtering has no effect to keep original shape of protrusions or rather reduces the height of protrusions especially when the sputter-power is as much as 200 W. The reason will be that the mass of nitrogen ion is much smaller than that of argon ion. In fact, according to preliminary experiments, the sputter-etching only by using nitrogen gas of 1.2 Pa at 100, 150, 200 W for 7.2 and 14 ks cannot form protrusions although the micro-Vickers hardness is largely increased by nitriding, e.g. from 243 of an original smooth specimen to 1014 of the specimen nitrided at 200 W for 7.2 ks.

3.2. X-ray diffraction analyses and optical micro-structures of protrusions

Fig. 3 shows X-ray diffraction patterns of typical three kinds of plasma-nitrided specimens. On the $N_2$130 Pa–50 W–14 ks specimen

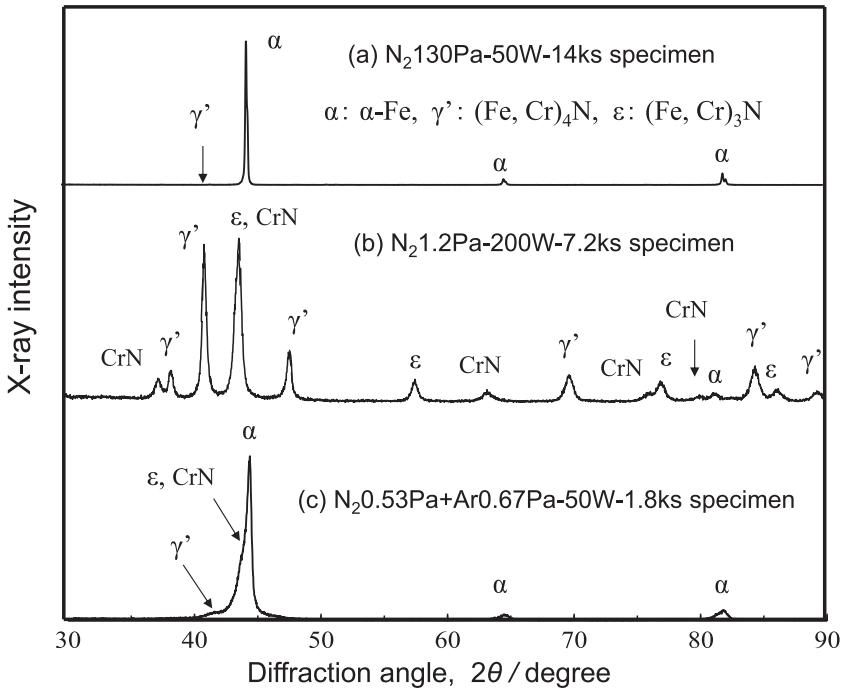

Fig. 3. X-ray diffraction peaks of $N_2$130Pa–50 W–14 ks specimen (a), $N_2$1.2 Pa–200 W–7.2 ks specimen (b) and $N_2$0.53 Pa–Ar0.67 Pa–50 W–1.8 ks specimen (c).

(a) there appears sharp diffraction peaks from α-phase (matrix) with a very small peak from γ′-(Fe, Cr)$_4$ N. On the $N_2$1.2 Pa–200 W–7.2 ks specimen (b), large peaks from ε-(Fe, Cr)$_3$ N, γ′-(Fe, Cr)$_4$ N and CrN phases are detected and there is only a small peak from α-phase. On the $N_2$0.53 Pa–Ar0.67 Pa–50 W–1.8 ks specimen (c), there are small peaks from the nitride phases with large peaks from α-phase. The broadening of the α-peaks compared with the peaks observed for the $N_2$130 Pa–50 W–14 ks specimen (a) suggests a large lattice distortion due to precipitation of nitrides. In addition, the diffraction angles from (110) plane of α-phase are 44.563° and 44.380° for the $N_2$130 Pa–50 W–14 ks (a) and the $N_2$0.53 Pa–Ar0.67 Pa–50 W–1.8 ks (c) specimens, respectively, which means the occurrence of lattice expansion due to a larger solution of nitrogen atoms for the $N_2$0.53 Pa–Ar0.67 Pa–50 W–1.8 ks specimen (c) than the $N_2$130 Pa–50 W–14 ks specimen (a).

Fig. 4 shows typical optical microstructures of cross-section of plasma-nitrided specimens. For the $N_2$130Pa–50 W–14 ks (a) and $N_2$0.53 Pa–Ar0.67 Pa–50 W–1.8 ks (e) specimens, the existence of nitride layer on the surface of protrusions is not obvious, although the X-ray diffraction analyses of Fig. 3(a) and (c) indicate the existence of a small amount of nitrides for both specimens. The protrusions seem to be composed of the diffusion layer α_N, where the super-saturated solid solution of nitrogen atoms occurs in α-phase accompanied by the precipitation of fine nitrides. The protrusion area is not etched even after a long time immersion into 5% nital solution, suggesting high corrosion resistance due to nitrogen solution [30,31]. The microstructure below the protrusion area will be a mixture of ferrite and chromium-iron double carbide, $(Cr, Fe)_mC_n$. The optical microstructure of the $N_2$1.2 Pa–50 W–7.2 ks specimen was the same as that of the above specimens.

Figs. 4(b) and 5(a) show microstructure and SEM image of the $N_2$1.2 Pa–200 W–7.2 ks specimen. These figures show that thick three nitride layers and underlying diffusion layer are formed, and the whole of protrusions is covered by the first layer. From the X-ray diffraction peaks in Fig. 3 and the analyses of other researches [21,29–31], it seems that the top layer is composed mainly of ε-(Fe, Cr)$_3$N. The second layer beneath the ε-layer will be mainly γ′-(Fe, Cr)$_4$N. The third layer will be a mixture of CrN and α-phase, and these three layers contain other kinds of nitrides. The fourth region is the diffusion layer composed of α-phase with solid-solution of N atoms and the precipitates along grain boundary as is shown in Fig. 5(b). Although detailed results are omitted, additional EDX analyses of the cross-section (Fig. 5(a)) showed that the distribution of chromium and nitrogen atoms exists in the depth direction, which supports that the nitride layers are composed of iron-chromium double nitrides, (Fe, Cr)$_x$N, and not a single iron nitride of Fe$_x$N. In addition, there are many particles with average sizes of about 1 μm in the nitride layers, and larger chromium and nitrogen contents than those of the (Fe, Cr)$_x$N matrix support the dispersion of CrN in the matrix. In addition, the precipitate along the grain boundary (point A in Fig. 5(b)) contains a larger amount of chromium and carbon than the region in grain, which corresponds to the precipitation of Cr(N, C) [31].

Figs. 4(c) and 5(c) show the microstructure and SEM image of the $N_2$1.2 Pa–100 W–1.8 ks specimen. There is only a single nitride layer, which is much different from those of the $N_2$1.2 Pa–200 W–7.2 ks specimen (Fig. 4(b)), corresponding to a lower surface temperature due to the lower nitriding power of 100 W. Chromium and nitrogen contents of the protrusion area were 12.2 and 4.9%, and those of the precipitate (Fig. 5, point B) were 24.6 and 7.5%, respectively. Although nitrogen content is qualitative in the preset EDX analysis, the protrusion is considered to be composed of ε-(Fe, Cr)$_3$N phase and CrN precipitates. The protrusions of the $N_2$1.2 Pa–(100, 200)W–1.8 ks specimens often contain cracks in the ε-(Fe, Cr)$_3$N layer, and such brittle protrusions cannot be used for mechanical purposes. Fig. 4(d) shows the microstructure of the $N_2$1.2 Pa–50 W–1.8 ks specimen, where the formation of ε-(Fe, Cr)$_3$N nitride layer is limited only to the surface region of the protrusion due to the lowest nitriding power of 50 W.

As is shown in Fig. 2(d), plasma-nitriding using high power of 200 W drastically decreased the sharpness of protrusions and the aspect ratio of height to diameter. In addition, the whole of the protrusions is composed of ε-(Fe, Cr)$_3$N nitride layer (Figs. 4(b), 5(a)), where the thickness of nitride layer that formed on the matrix around the protrusions is much smaller than the height of the protrusions. It is possible that high speed impingement of nitrogen atoms to the protrusion surface under high nitriding power has resulted in a much higher temperature of the protrusions than the matrix surface. The high temperature has not only accelerated the formation of nitrides on the protrusions but also facilitated nitrogen ion sputtering of the protrusions rather than the matrix around the protrusions, which has reduced the height of the protrusions. On the other hand, when the nitriding power is 50 W

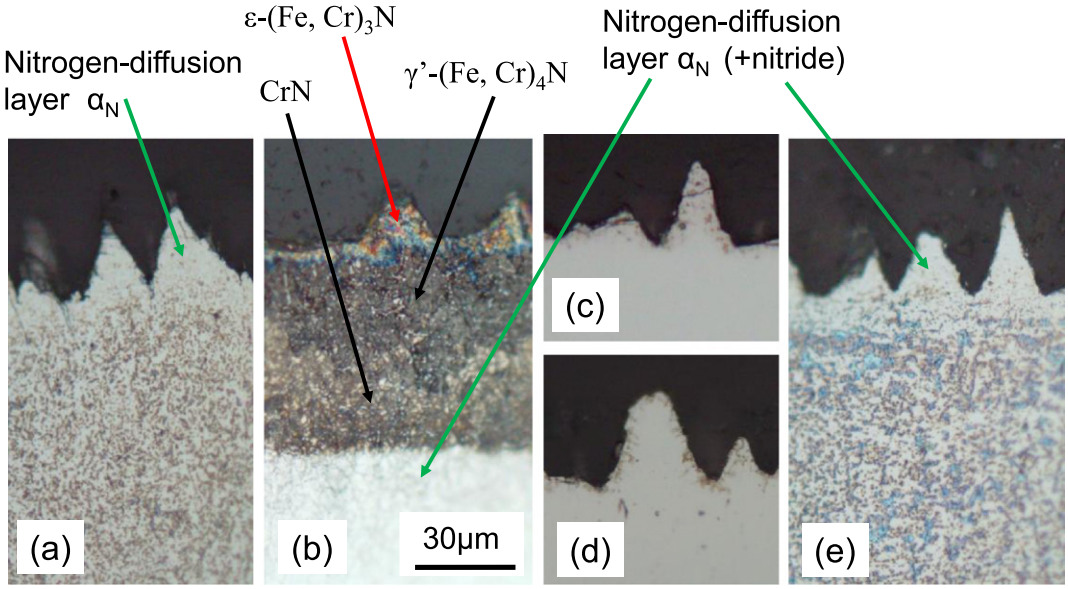

Fig. 4. Optical microstructures of $N_2$130Pa–50 W–14 ks (a), $N_2$1.2 Pa–200 W–7.2 ks ks (b), $N_2$1.2 Pa–100 W–1.8 ks (c), $N_2$1.2 Pa–50 W–1.8 (d) and $N_2$0.53 Pa–Ar0.67 Pa–50 W–1.8 ks (e) specimens. Scales are all the same.

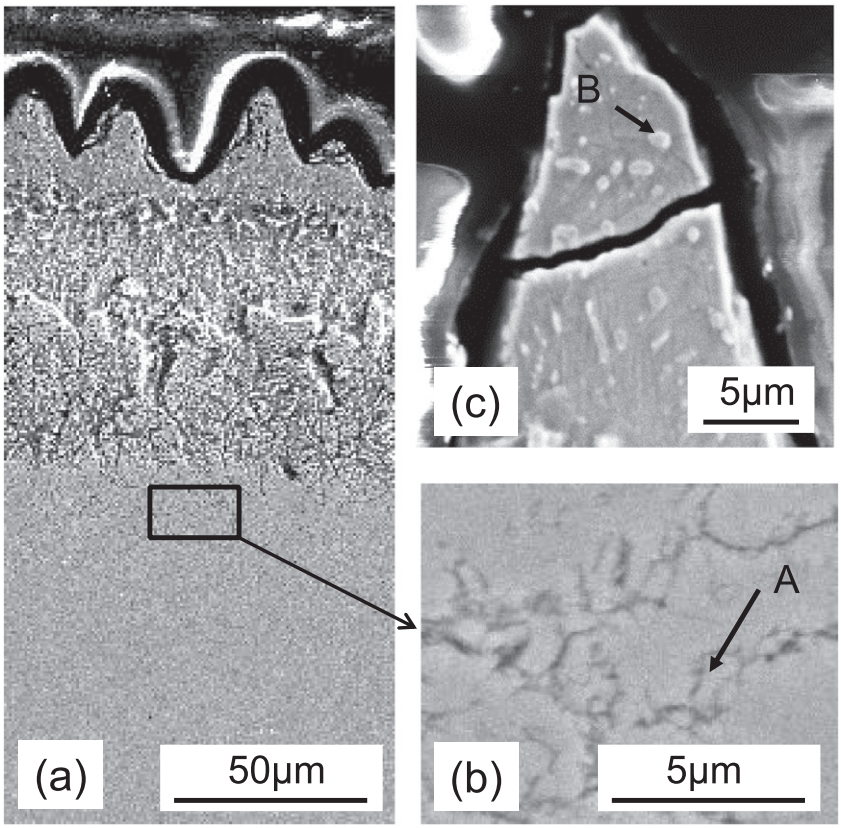

Fig. 5. SEM images of $N_2$1.2 Pa–200 W–7.2 ks specimen (a) with enlargement of nitrogen diffusion region (b), and N_2 1.2 Pa–100 W–1.8 ks specimen (c). Points A and B are Cr(N, C) and CrN precipitates.

(Figs. 2(b), 4(d)), the impingement of nitrogen ions with moderate speed seems to have prevented the surface from large increase in temperature and formation of thick nitride layer keeping the original sharpness of protrusions with small sputtering effect.

3.3. Deformation resistance of protrusions to indentation force

In order to obtain the information on the compressive strength of protrusions when they are used as a surface of transcription roll, micro-Vickers hardness tests were carried out at an indentation force of 2.9 N. Indentation was carried out to several protrusions together because it was difficult to make the indentation exactly on the top of a protrusion. Fig. 6 shows examples of SEM top images of the deformation observed for the as-sputter-etched specimen (a), $N_2$130Pa–50 W–14 ks specimen (b), $N_2$1.2 Pa–200 W–7.2 ks specimen (c) and $N_2$0.53 Pa–Ar0.67 Pa–50 W–1.8 ks specimen (d), respectively. The protrusions that were pushed by the center part of the pyramidal indenter were heavily deformed, whereas the protrusions apart from the center were pushed down aside by the side surface of the indenter. According to Fig. 6, the deformation of protrusions of as-sputter-etched specimen (a) is large. On the other hand, that of $N_2$1.2 Pa–200 W–7.2 ks specimen (c) with nitride layer and blunt top is small but there exist vertical cracks on the protrusions, i.e. the protrusions are hard but brittle due to the formation of ε-nitride (Fig. 4(b)). On the contrary, the protrusions of $N_2$130Pa–50 W–14 ks specimen (b) and $N_2$0.53 Pa–Ar0.67 Pa–50 W–1.8 ks specimen (d) have no cracks and are more ductile than those of $N_2$1.2 Pa–200 W–7.2 ks specimen corresponding to the structures without brittle nitride layers (Fig. 4(a) and (e)).

Fig. 7 shows the comparison of indentation resistance of the protrusions (average of more than seven test results for each specimen) defined as, $\sigma_i = F/S$, where F is the indentation force (2.9 N) and S ($=a \times a$) is the square area within which the deformation of protrusions is observed (refer to the square flame in Fig. 6(c), (d) and in Fig. 7). According to Fig. 7, the σ_i of $N_2$130Pa–(50, 100)W–7.2 ks specimens in group 1 are almost the same as that of the as-sputter-etched specimen. A relatively large increase in the σ_i is obtained when the nitriding time is prolonged to 14 ks, i.e. the σ_i of the $N_2$130Pa–50 W–14 ks specimen is about 1.3 times larger than that of the as-sputter-etched specimen. Because the nitrides are scarcely detected from the X-ray diffraction analysis (Fig. 3(a)), strength mechanism of this specimen will be solution hardening.

The protrusions of $N_2$1.2 Pa–50 W–(1.8, 3.6, 7.2)ks specimens in group 2 revealed about 1.4 times larger indentation resistances than that of the as-sputter-etched specimen. On the other hand, the $N_2$1.2 Pa–100 W–(1.8, 7.2)ks specimens revealed almost twice larger indentation resistance than that of as-sputter-etched specimen. However, the protrusions of the $N_2$1.2 Pa–100 W–7.2 ks specimen are not sharp (Fig. 2(c)) and the $N_2$1.2 Pa–100 W–1.8 ks specimen is deformed with many cracks at the indentation test (Fig. 7). The indentation resistance of the $N_2$1.2 Pa–200 W–7.2 ks specimen is three times as large as that of as-sputter-etched specimen, but the tip of the protrusion is dull (Fig. 2(d)). Because the whole of the protrusions and the region under the protrusion of this specimen are composed of nitrides (Figs. 4(b), 5(a)), the resistance and deformation behaviors of protrusions are those of nitrides. Although it may be possible to find an optimum nitriding condition to increase the resistance of the protrusions without formation of thick nitride layer even at a low nitrogen pressure by changing the combinations of nitriding power and time, plasma-nitriding using only nitrogen gas has a fatal limitation in that the sputter effect of nitrogen ions always reduces the sharpness and height of protrusions.

The $N_2$0.53 Pa–Ar0.67 Pa–50 W–1.8 ks specimen in group 3 gives 1.9 times larger indentation resistance than that of the as-sputter-etched specimen with very short nitriding time of 1.8 ks keeping the sharpness

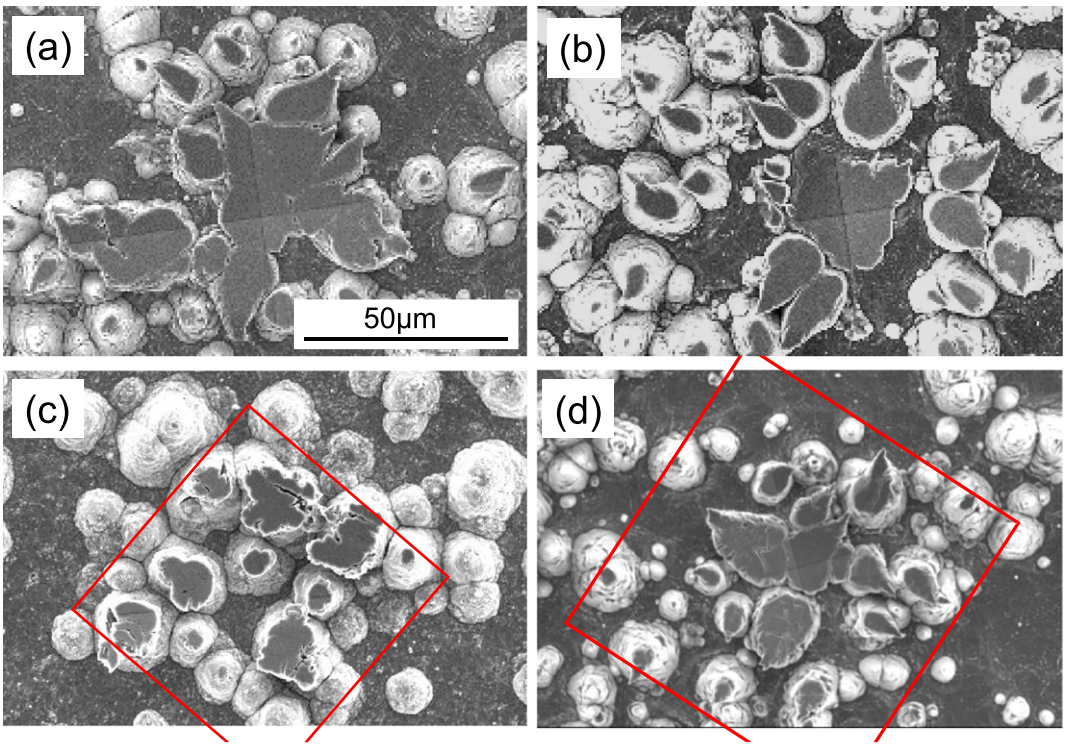

Fig. 6. Deformation of protrusions after application of indentation force of 2.9 N: As sputter-etched specimen (a), $N_2$130 Pa–50 W–14 ks specimen (b), $N_2$1.2 Pa–200 W–7.2 ks specimen (c) and $N_2$0.53 Pa + Ar0.67 Pa–50 W–1.8 ks specimen (d). Scales are all the same.

of the protrusions (Fig. 2(e)). Because there are small diffraction peaks of nitrides in the X-ray analysis (Fig. 3(c)) and no observable nitride layers in the microstructure (Fig. 4(e)), the strengthening mechanism is due to both solution hardening and precipitation hardening. The $N_2$0.53 Pa–Ar0.67 Pa–50 W–7.2 ks specimen shows almost the same strength in spite of four times longer nitriding time. This suggests that the argon ion sputtering at 0.67 Pa stably removes the nitride layer formed by excess solution of nitrogen at 0.53 Pa without removing the nitrogen diffusion layer, and this balance is almost kept at least during 1.8 to 7.2 ks. If the pressure of mixed argon gas was much larger than that of the nitrogen gas, the hardening would not occur even if the sharpness of the protrusions is maintained. This balance also depends on the power even if the mixing rate is the same: as is shown in Table 1, the SEM images showed that the sharpness of the $N_2$0.53 Pa–Ar0.67 Pa–100 W–1.8 ks specimen was barely kept but that of the $N_2$0.53 Pa–Ar0.67 Pa–200 W–1.8 ks specimen was completely lost. Thus, at high power of 100 and 200 W, the nitriding effect overcomes the sharpening effect by argon sputter-etching.

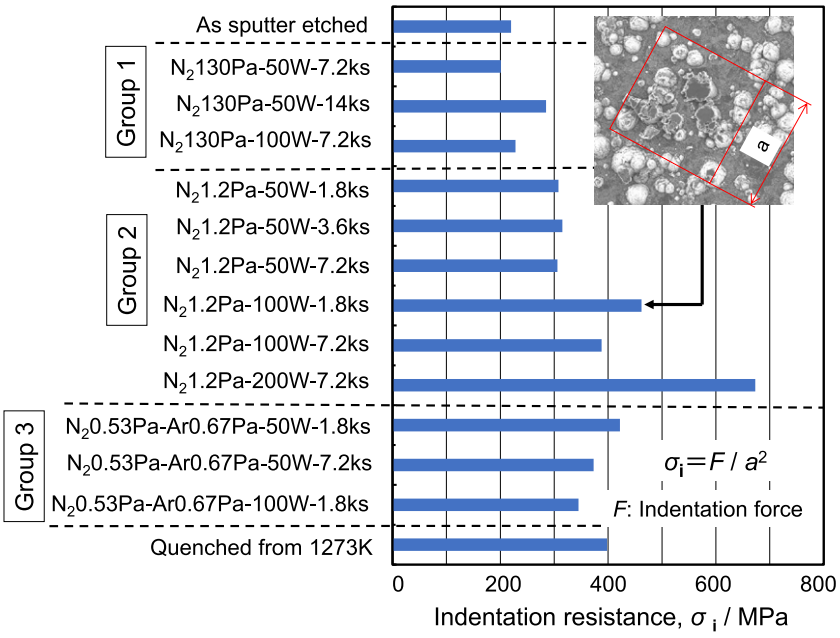

Fig. 7. Comparison of indentation resistances of plasma-nitrided protrusions ($F = 2.9$ N).

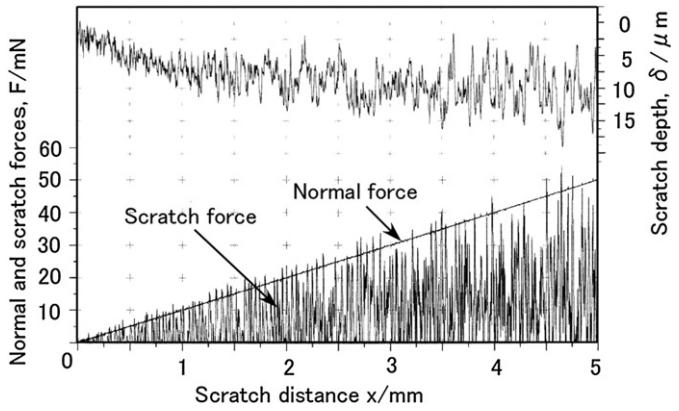

Fig. 8. Relationships between scratch distance and normal force, scratch force and scratch depth obtained for as-sputter-etched specimen (250 W for 9 ks).

The reason for a larger strength achieved in the $N_2$0.53 Pa–Ar0.67 Pa–50 W–1.8 ks specimen than that in the $N_2$130Pa–50 W–14 ks specimen within much shorter time of 1.8 ks can be attributed to two effects. One is that the argon gas mixed into nitrogen gas has activated the entry of nitrogen into the protrusions by sputter-cleaning (sputter-etching) of protrusion surface. Another is that a longer mean free path or high impingement velocity of nitrogen ions under the much smaller nitrogen gas pressure of 0.53 Pa than 130 Pa has facilitated the solution of nitrogen atoms to the protrusion. Fig. 7 also shows the indentation resistance σ_i measured for the protrusions of quenched specimen previously reported [20]. The $N_2$0.53 Pa–Ar0.67 Pa–50 W–1.8 ks specimen has almost the same strength as that of the quenched specimen.

3.4. Deformation resistance of protrusions to scratch force

The protrusions on a traction roll receive tangential or lateral force. In order to evaluate the resistance of protrusions to the lateral force, nano-scratch tests were carried out on three positions per one sample under a constant normal loading speed of 0.17 mN/s. Fig. 8 shows a typical relationship between scratch distance and both scratch (frictional) force and scratch (penetration) depth obtained for the as-sputter-etched specimen. Fig. 9 shows the SEM images of the scratch track after the test, which indicates that the protrusions were pulled down by scratch with large plastic deformation. According to Fig. 8, scratch forces largely vary from zero to peak values corresponding to discontinuous contacts of the indenter tip to randomly distributed protrusions with different intervals and heights. The peak values do not necessarily correspond to the forces applied right back of protrusions because in some cases the scratch tip passes thorough only deforming the side of protrusions as are observed in Fig. 9. The scratch depth also changes largely but it does not necessarily returns to zero because the tip is automatically controlled to keep contact to the protrusions to maintain constant load, whereas a maximum depth value sometimes corresponds to a direct scratch of the matrix where there is no protrusion. Thus, in the present research, the average scratch depth at the scratch distance of 5 mm (at the end of test), δ_5, is adopted as a measure of the deformation resistance of protrusion(s) to a vertical force. The δ_5 corresponds to the indentation resistance σ_i obtained by the micro-Vickers test discussed above although the contact is limited only to a few protrusions in the scratch test. At the end of the test the scratch tip almost reaches the bottom of a protrusion (Fig. 9), where the peak scratch force is about 55 mN and the average scratch tip depth, δ_5, is about 10 μm (Fig. 8).

Fig. 10 shows the scratch track observed for the $N_2$1.2 Pa–200 W–7.2 ks specimen. Nitrided protrusions are broken with brittle manner without plastic deformation. The scratch tip does not reach the bottom of the protrusion at the end of the test (Fig. 10(d)) and the average scratch tip depth, δ_5, was about 5 μm. These facts mean that the protrusions of the $N_2$1.2 Pa–200 W–7.2 ks specimen are brittle but they are so hard that the indenter is difficult to move down to the matrix at the end of test, and the scratch resistance when the fracture occurs at the bottom section of the protrusion is not obtained.

Fig. 11 shows the scratch track of the $N_2$0.53 Pa–Ar0.67 Pa–50 W–1.8 ks specimen at the end of test (scratch distance of 5 mm), where the separation of the top part occurs with some degree of plastic

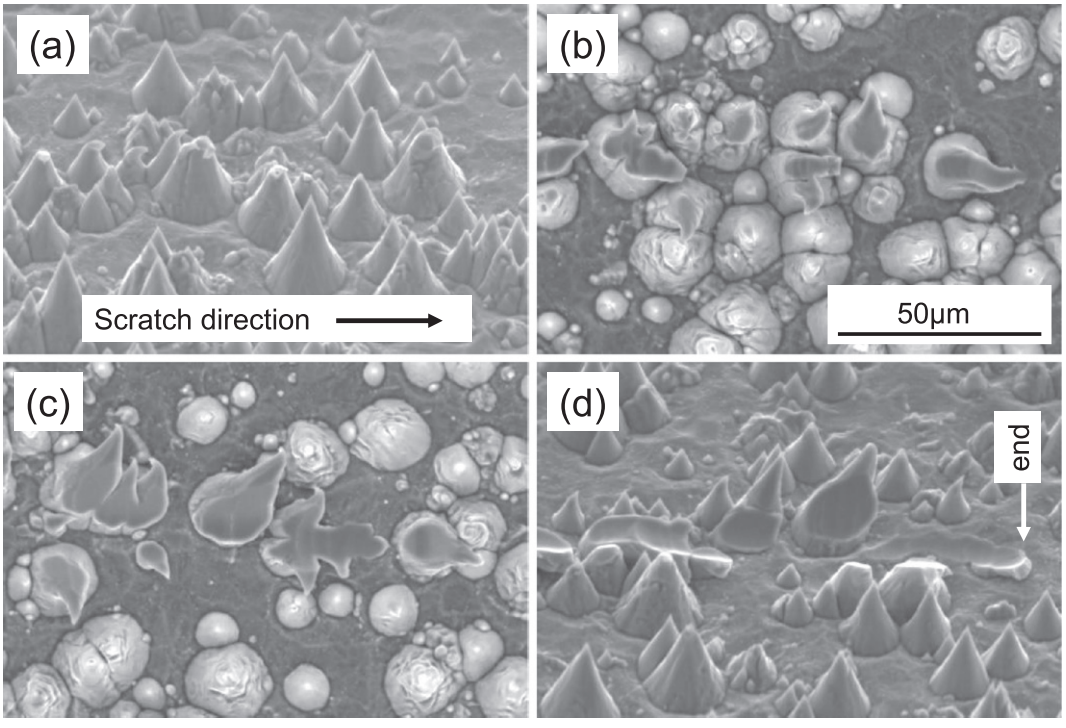

Fig. 9. Scratch deformation of protrusions of as-sputter-etched specimen. (a) and (d) are 45° inclined side views, and (b) and (c) are top views. Scales are all the same.

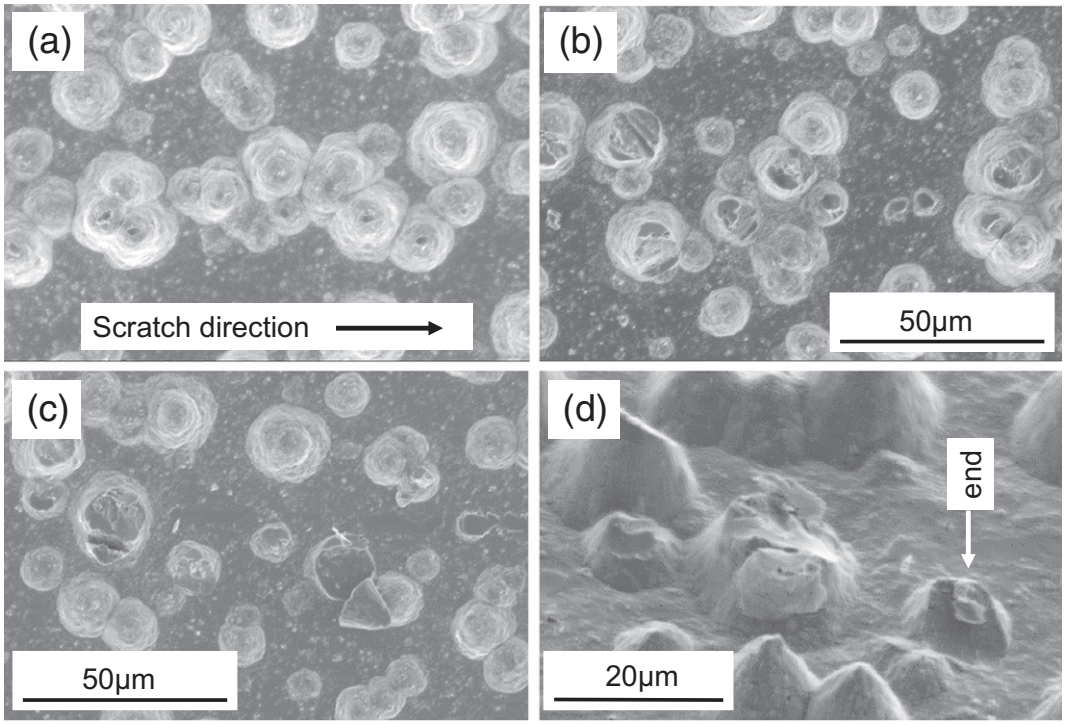

Fig. 10. Scratch deformation of protrusions of $N_2$1.2 Pa–200 W–7.2 ks specimen. (a), (b) and (c) are top views, and (d) is 45° inclined side view.

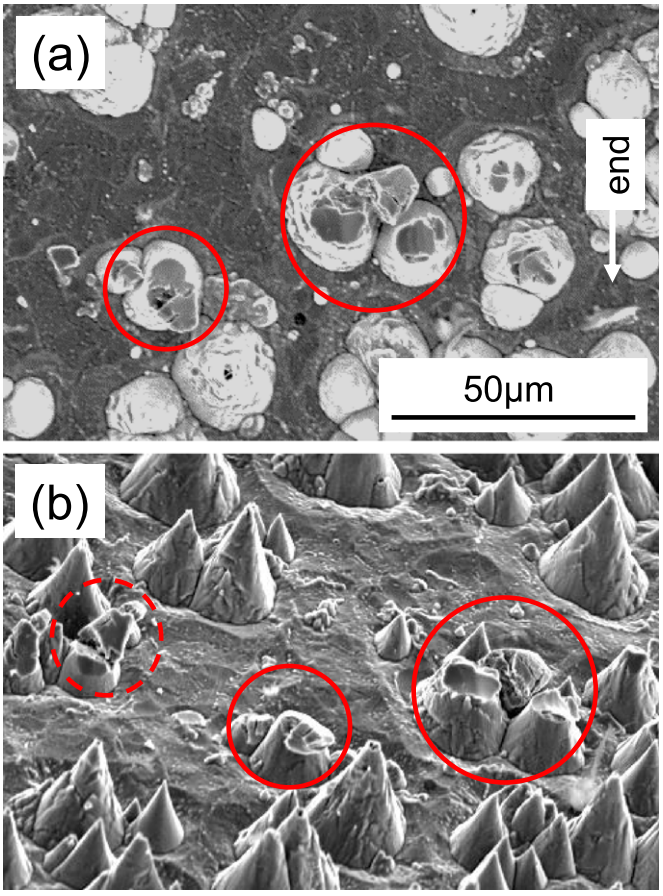

Fig. 11. Scratch deformation of protrusions of $N_2$0.53 Pa–Ar0.67 Pa–50 W–1.8 ks specimen at the end of test. (a) is top view and (b) is 45° inclined side view.

deformation. The maximum scratch strength and the average scratch depth at the end of the test, δ_5, were 57 mN and 7.2 μm, respectively. Also in this case, the scratch tip does not reach the matrix at the end of the test. The maximum or true scratch resistance of individual conical protrusion is obtained only when the scratch tip contacts the bottom of the protrusion, so that if the scratch tests of the $N_2$0.53 Pa–Ar0.67 Pa–50 W–1.8 ks and $N_2$1.2 Pa–200 W–7.2 ks specimens were carried out to a longer scratch distance than 5 mm much larger scratch resistances of protrusions would be obtained. When there is no such data, the scratch resistances of the protrusion measured at the same scratch depth will give a comparison of each specimen.

Fig. 12 shows a comparison of maximum scratch forces obtained at the same scratch depth of 5 μm, F_5, for the above three specimens. This figure also shows the average scratch depth at the end of test, δ_5. The scratch resistance F_5 is the largest for the $N_2$1.2 Pa–200 W–7.2 ks specimen although the top of the protrusions is dull and the cross-section is a little larger at the same distance from the top of the protrusion. On the other hand, the $N_2$0.53 Pa–Ar0.67 Pa–50 W–1.8 ks specimen reveals a lower resistance than the $N_2$1.2 Pa–200 W–7.2 ks specimen but a higher resistance than the as-sputter-etched specimen. The scratch depth at the end of the test, δ_5, is the smallest for the $N_2$1.2 Pa–200 W–7.2 ks specimen, and it is still smaller for the $N_2$0.53 Pa–Ar0.67 Pa–50 W–1.8 ks specimen than the as-sputter-etched-specimen. These tendencies are similar to the results of micro-Vickers tests shown in Fig. 7.

The above indentation and scratch tests show that the $N_2$1.2 Pa–200 W–7.2 ks specimen has the largest indentation and scratch resistances. However, the protrusions of this specimen are composed of brittle ε-$(Fe, Cr)_3N$ nitride often including inherent cracks, so that the reliability will be small when they are used as a machine part receiving impact bending or scratch force. Therefore another measure expressing the toughness, or an appropriate combination of strength and ductility, of a protrusion is necessary to confirm the practical applicability of the protrusions. Although the deformation of the protrusions is more clearly observed after the scratch test than the indentation test, the deflection until the separation of the top part of protrusion cannot be measured in the present nano-scratch test. So that the degree of plastic deformation before the separation of the top part of the protrusion, i.e.

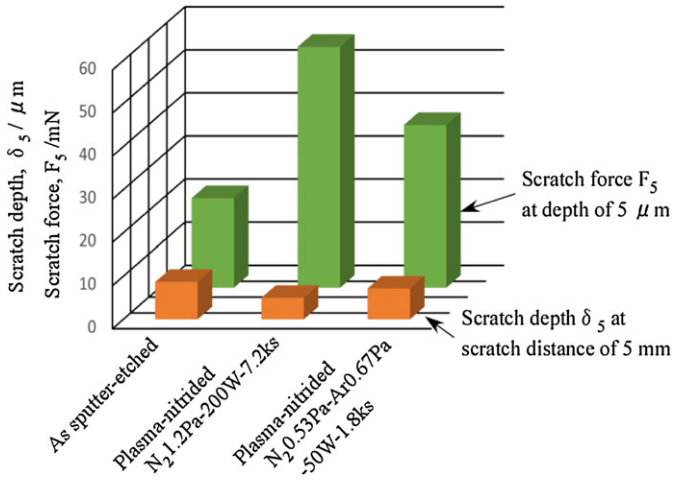

Fig. 12. Comparison of scratch force at scratch depth of 5 μm and scratch depth at scratch distance of 5 mm.

deformation appearance, is adopted as a qualitative measure of ductility and defined as "scratch ductility". Because the nano-scratch tests were carried out only for three specimens, additional SEM observations were carried out on other specimens along a needle scratch track that was prepared as a marker line for indentation tests. Fig. 13 shows examples of deformation appearance of protrusions. The top parts of the protrusions of the $N_2$130Pa–50 W–7.2 ks (a) and $N_2$1.2 Pa–50 W–7.2 ks (b) specimens are separated after large plastic deformation or still remain, i.e. the scratch ductility is very large, whereas the top parts of the protrusions of the $N_2$1.2 Pa–100 W–7.2 ks specimen (c) are separated with brittle manner with small plastic deformation, i.e. the scratch ductility is low. The "scratch ductility" is ranked from A–D for all the specimens on the bases of deformation appearance and are summarized in Table 1.

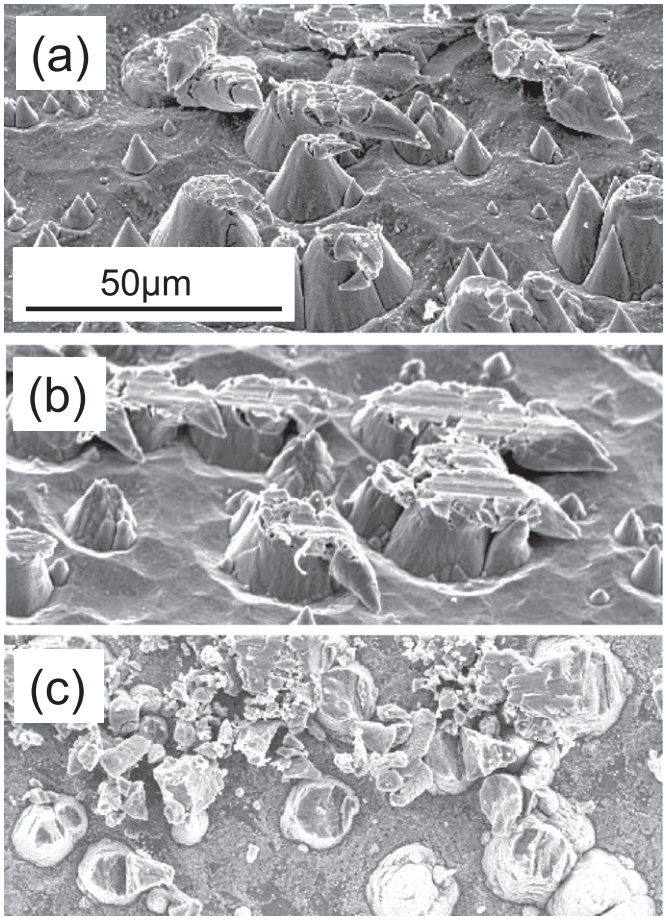

Fig. 13. Scratch deformation of protrusions of $N_2$130 Pa–50 W–7.2 ks (a), $N_2$1.2 Pa–50 W–7.2 ks (b), $N_2$1.2 Pa–100 W–7.2 ks (c) specimens along marker lines. (a) and (b) are 45° inclined side views and (c) is top view. The scales are all the same.

Considering some correspondence between the scratch resistances obtained from nano-scratch tests shown in Fig. 12 and the indentation resistances shown in Fig. 7, the toughness of the protrusions can be evaluated by a combination of deformation resistances and scratch ductility. For example, the toughness of the $N_2$1.2 Pa–200 W–7.2 ks protrusions is very small because the scratch ductility is too small in spite of the largest resistances. On the other hand, the toughness of the $N_2$0.53 Pa–Ar0.67 Pa–50 W–1.8 ks protrusions is large because both the resistances and scratch ductility are moderate. The toughness of the as-sputter-etched protrusions is also small because the deformation resistance is small although the scratch ductility is very large. However, it does not necessarily mean that the protrusions of as-sputter-etched specimen cannot be applied to the traction and transcription rolls because the protrusions are sharp enough and not brittle. Their applicability depends on the hardness of sheet materials to be transported.

It is understood from the experimental results shown in Table 1, Figs. 7 and 12 that the plasma-nitriding using a mixture of nitrogen and argon gases at 50 W is an optimum condition to increase indentation and scratch resistances as well as toughness of protrusions within a short time of 1.8 ks keeping sharpness of protrusions without forming brittle and thick nitride layers on the protrusion surface.

4. Conclusions

Argon ion sputter-etching of AISI type 420 martensitic stainless steel was carried out to form conical protrusions with bottom diameter of 10–30 μm on the specimen surface. Plasma-nitriding was carried out on the protrusions by changing nitrogen gas pressure, nitriding power, time and mixing rate of nitrogen and argon gases. Deformation resistances of the nitrided protrusions were measured by micro-Vickers and nano-scratch tests. The results obtained are as follows.

(1) When the nitrogen gas pressure is 130 Pa and the nitriding power is 50 W, there is no observable nitride layer on the surface of the protrusions and the top of the protrusions is sharp. However, the indentation resistance of the protrusion is about 1.3 times as large as that of the as-sputter-etched specimen even after 14 ks nitriding.

(2) Plasma-nitriding of protrusions using a lower nitrogen gas pressure of 1.2 Pa at higher nitriding power of 200 W for 7.2 ks has resulted in the formation of the nitride layers covering the whole of protrusions. Although the protrusions have almost three times higher indentation and scratch resistances than those of the as-sputter-etched specimen, they are brittle and the sharpness of each protrusion is lost. When the nitriding power is decreased to 50 W, the sharpness of the protrusions is recovered but the indentation resistance of the protrusion is only 1.4 times as large as that of the as-sputter-etched specimen.

(3) Plasma-nitriding using a mixture of nitrogen gas of 0.53 Pa and argon gas of 0.67 Pa at the low nitriding power of 50 W for 1.8 ks produces almost twice larger indentation and scratch resistances than those of the as-sputter-etched specimen. This is one of the optimum conditions to increase not only the resistances but also the toughness of the protrusions within a short time, keeping the sharpness of protrusions without forming brittle and thick nitride layers on the protrusion surface. It is considered that the sputtering by mixed argon ions not only promotes the solid solution of nitrogen but also prevents the formation of thick nitride layer on protrusion surface.